Nonlinear-resonance analysis of halo formation excited by beam-core oscillation

Yoshito Shimosaki
Department of Energy Science and Engineering, Kyushu University, Fukuoka 812-8581, Japan

Ken Takayama
Accelerator Laboratory, High Energy Accelerator Research Organization (KEK), Tsukuba, Ibaraki 305-0801, Japan

(Received 13 October 1999)

The emittance growth and halo formation for a mismatched beam of a one-dimensional Gaussian distribution in a uniform focusing channel were examined by means of a macroparticle simulation. The results were analyzed by isolated nonlinear resonance theory. The second-harmonic resonance driven by beam-core oscillation was both numerically and analytically shown to assume a key role in forming a halo. An analytic estimation of the halo location was explored, and the halo location was proved to correspond to the outer edge of the resonance islands. Nonlinear fields in an actual particle distribution have been shown to significantly affect both the halo's location and size.

PACS number(s): 41.75.−i, 29.27.Bd, 52.25.Wz

I. INTRODUCTION

One of the major issues in high-power accelerators for neutrino factories, spallation neutron sources, tritium production, nuclear waste transformation, and heavy ion fusion drivers is the activation of accelerator components due to beam loss. The beam loss must be reduced to a suffuciently low level to allow hands-on maintenance. The loss rate commonly accepted in accelerator society is known to be 1 W/m, except for specified regions, such as the halo-collimation region. In order to produce an acceptable design, it is important to understand the mechanisms of emittance growth and halo formation that result in beam loss.

Most of the recent attention has been focused on driver linacs. Totally self-consistent particle in cell simulation (PIC) codes have been developed, which have demonstrated a wide variety of aspects of halo formation for realistic beam distributions [1]. Meanwhile, the analysis and understanding of space-charge effects for particle beams in linacs has been greatly facilitated by using particle core models (PCMs). As the driving mechanism of halo formation, a resonant (parametric) interaction between the breathing core and the individual particles oscillating through the beam core has been explored using this model by many research groups [1–3]. Certainly, PCMs are useful for developing a qualitative understanding of the halo-formation mechanism, and the explored mechanisms are suggestive for a more realistic distribution as mentioned in Ref. [3]. However, there is no confidence that we are capable of quantitatively estimating the size of a halo and its parameter dependence.

In contrast to the case for linacs, an understanding of halo-formation mechanisms in circular rings seems to be quite difficult even when using PIC codes with realistic distribution, because numerical calculations over a sufficient number of turns require unrealistic CPU times and memory and repeated betatron oscillations through a huge number of lattice elements take a key role in the resonant interaction. We have pursued a strategy to develop a useful analytic model capable of predicting the position of the halo as a function of the beam and machine parameters for a realistic beam distribution. As the first step of this strategy, halo formation in a one-dimensional (1D) Gaussian distribution in a uniform focussing channel has been numerically examined, and a second-harmonic nonlinear resonance excited by the rms core oscillation has been identified to be a driving mechanism of halo formation. This view has been confirmed by an analytic approach based on isolated nonlinear resonance theory [4,5]. The simulation and theory have shown that highly nonlinear components in real distribution strongly affect the halo location. The current analytic approach is believed to be a germinal model in future theory dealing with a 2D realistic distribution in the FODO lattice.[1]

The organization of this paper is as follows. In Sec. II, we present a model of a 1D multiparticle simulation. The developed simulation is justified by a comparison with an equilibrium solution of Vlasov's equation. In Sec. III, three cases of a mismatched space-charge-dominated beam are discussed based on this simulation model. The isolated resonance Hamiltonian is applied to explain the simulation results in Sec. IV. In Sec. V, the obtained results are summarized.

II. MULTIPARTICLE SIMULATION

First of all, we describe a 1D simulation method which was used to understand the detailed and dynamic processes involved in the physical phenomena. In the simulation, a beam distribution is assumed to be both infinite and uniform in the horizontal and longitudinal planes and finite and nonuniform in the vertical plane. Space-charge fields affect the betatron motion of the beam in the vertical direction. In addition, it is assumed that the beam propagates through free space so that the effect of the image charge is ignored.

The electric field originating from the beam space charge in the rest frame (where x, y, and s represent the horizontal, vertical, and longitudinal axes, respectively) is written as

$$E_y(y) = \frac{e}{2\epsilon_0}\left[\int_{-\infty}^{y} n(q)dq - \int_{y}^{\infty} n(q)dq\right], \qquad (2.1)$$

[1]FODO is an array of magnets where F is focusing, D is defocusing, and O is the drift space between magnets.

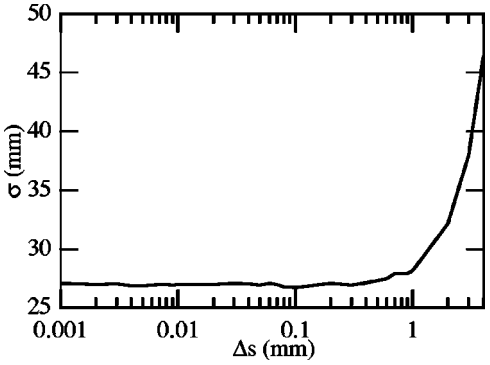

FIG. 1. σ vs Δs. Step-size dependence of simulation results. Here (σ) is rms beam size after one turn.

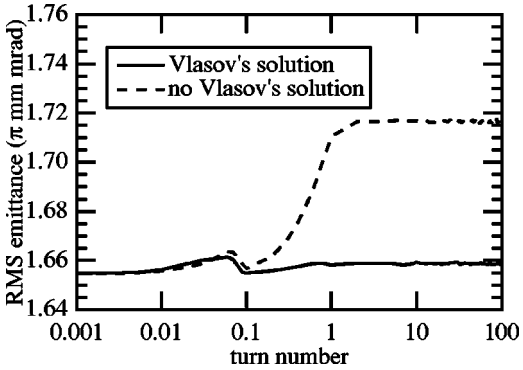

FIG. 2. rms emittance growth.

where $n(y)$ is the particle-density function in the rest frame and ϵ_0 is the permittivity of the vacuum. The space-charge forces in the laboratory frame are written as $F_y(y) = eE_y(y)/\gamma$, where γ is the relativistic mass factor. If the particle energy is constant, the betatron equation is given by

$$y'' + \omega_\beta^2 y = \frac{eE_y(y)}{\gamma^2 m v^2}, \tag{2.2}$$

where the prime indicates d/ds, ω_β is the bare betatron frequency, and v is the velocity of the design particle. In general, $E_y(y)$ is nonlinear with respect to y. The perturbing effects of nonlinear fields are included as δ functions like kicks [6],

$$\begin{pmatrix} y_{s+\Delta s} \\ y'_{s+\Delta s} \end{pmatrix} = M \begin{pmatrix} y_s \\ y'_s \end{pmatrix} + \begin{pmatrix} 0 \\ \dfrac{eE_y(y_{s+\Delta s})}{\gamma^2 m v^2} \Delta s \end{pmatrix}, \tag{2.3}$$

where M is the transfer matrix of the linear focusing system and Δs is the longitudinal step. The electric field, which is assumed to be constant through Δs, is measured at the exit of step. In this way, the symplectic condition is satisfied.

The space-charge fields depend on $n(y)$ as shown in Eq. (2.1) and its magnitude changes bin by bin. At the exit of the step, $n(y)$ is calculated by using the histogram obtained from the phase-space mapping of particles with the vertical bin Δy. The numerical integration of $n(y)$ with linear interpolation gives a space-charge field.

We chose to apply the current study to the 12-GeV proton synchrotron (KEK-PS). Most of the calculation parameters were taken from the KEK-PS, where $C = 340$ m is the circumference, the bare tunes are $\nu_x = 7.15$ and $\nu_y = 6.23$, where $2\pi\nu_y = \omega_\beta C$, and the injection energy is 500 MeV. In order to manifest the key role of the space-charge effects in halo formation, an extremely high current, $\Delta\nu = 1.85$, was studied, where $\Delta\nu = [\omega_\beta - \sqrt{\omega_\beta^2 - e^2\langle n_0\rangle\gamma^{-2}\epsilon_0^{-1}m^{-1}v^{-2}}]C/(2\pi)$ is the incoherent tune shift. In simulations, 10^5 macroparticles, which were chosen from the limit of the available CPU, were tracked for more than 100 turns. For choosing Δs, the saturation of the rms beam size σ of the simulation result was monitored as a function of Δs (see Fig. 1). As a result, $\Delta s = 5$ cm was applied. The value of Δy is a common parameter for both histogram and numerical integration. A Δy too short is very sensitive to noise and a Δy too large gives a very discrete distribution in the histogram. It has turned out that Δy = (full beam size)/100 provides sufficient accuracy.

To justify the simulation scheme, we think in terms of an equilibrium state which has an analytic solution under the space-charge effects. Vlasov's equation tells us that any equilibrium distribution function f is a function of the Hamiltonian H. As an example, the Gaussian distribution is $f(y,p) = f_0 \exp(-H/H_0)$, where f_0 is the value at the origin in phase space and H_0 is a normalizing function, and the Hamiltonian is written as

$$H = \frac{1}{2}p^2 + \frac{\omega_\beta^2}{2}y^2 + \frac{eU}{\gamma m v^2}. \tag{2.4}$$

Then, the self-potential satisfies Poisson's equation $\nabla^2 U = -en(y)/\epsilon_0$. The density function is obtained by integrating $f(H)$ over momentum space: $n(y) = n_0 \exp[-\{(\omega_\beta y)^2/2 + eU/(\gamma m v^2)\}/H_0]$ and $n_0 = \sqrt{2\pi H_0} f_0$ The electric field for the equilibrium state is dominated by the equation

$$\frac{\partial E_y}{\partial y} = \frac{en_0}{\epsilon_0} \exp\left[-\frac{1}{H_0}\left(\frac{\omega_\beta^2}{2}y^2 - \frac{e}{\gamma m v^2}\int_0^y E_y dy \right) \right]. \tag{2.5}$$

Numerically solving Eq. (2.5), we have $E_y(y)$; then, its numerical integration gives a steady potential $U(y)$. Substituting $U(y)$ into Eq. (2.4), we have an equilibrium Gaussian distribution function $f(H)$. This exact equilibrium Gaussian distribution was put into the calculation as an initial condition of the simulation. The simulation results are shown in Fig. 2. The rms emittance does not change much, with growth of less than 0.3%. For a comparison, an exact equilibrium Gaussian distribution function without any space-charge effects was calculated. The growth of its rms emittance is shown in the same figure. Its rms emittance quickly saturates with a big growth of about 4%. The discrepancy between the two cases is quite clear. Thus, the simulation scheme has been confirmed to give a reasonable result.

III. STEADY STATES FOR MISMATCHED GAUSSIAN, WATERBAG, AND SQUARE-COSINE DISTRIBUTIONS

We now call a beam having an exact equilibrium distribution function with space-charge effects as a ''matched

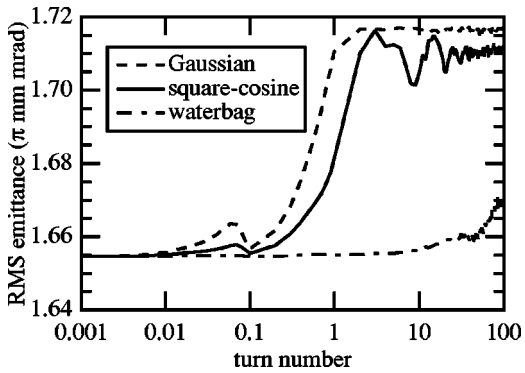

FIG. 3. rms emittance growth of the mismatched beams.

beam'' and other beams as ''mismatched beams.'' The simulations were carried out for three cases of mismatched beams with Gaussian, waterbag, and square-cosine distributions. The square-cosine distribution is defined as $f(y,y')=f_0\cos^2[\pi\sqrt{y^2+y'^2}/\{2R(y,y')\}]$, where $R(y,y')$ is the distance from the origin to the outer edge through (y,y') in phase space. Notable features are that the profile is continuous at the beam boundary like that of a Gaussian distribution, and the beam edge is finite like that of a waterbag distribution. All initial distribution functions have the same total current and the same rms emittance as the matched beam.

The rms emittance growth of the mismatched beams is shown in Fig. 3. Gaussian and square-cosine distributions quickly arrive at the steady state after less than a few tens of turns ($\leqslant 3$ for Gaussian and $\leqslant 30$ for square-cosine), whereas the rms emittance of the waterbag beam still grows over 1200 turns (see Fig. 4). The beam density of each distribution is shown in Fig. 5. It is found that a beam with an initial square-cosine distribution approaches a Gaussian distribution in the steady state. On the other hand, a beam with a waterbag distribution tends to become flat because of redistribution towards the beam edge.

The phase-space projections are shown in Fig. 6, and suggest that particles escaping from the core are responsible for the growth of rms emittance. In addition, it is remarkable that there are two vacant regions where particles do not exist. This particle redistribution seems to originate from nonlinear resonances. Ten test particles were put in one vacant region for the square-cosine distribution [see Fig. 7(a)] and tracked for another 100 turns. The oscillation frequency spectra obtained by fast Fourier transform (FFT) are shown in Fig. 7(b), where the particles are numbered from the beam core edge toward the outside. All spectra indicate sharp peaks, where $\nu_\beta=5.23$ is the net betatron tune depressed by space-charge forces. For a comparison, the oscillation frequency spectra for nonresonant particles are shown in Figs. 7(c) and 7(d). The oscillation frequency simply depends on the oscillation amplitude because of the nonlinear space-charge fields. This means the motions of the test particles are dominated by nonlinear resonances and the vacant region corresponds to the resonance islands.

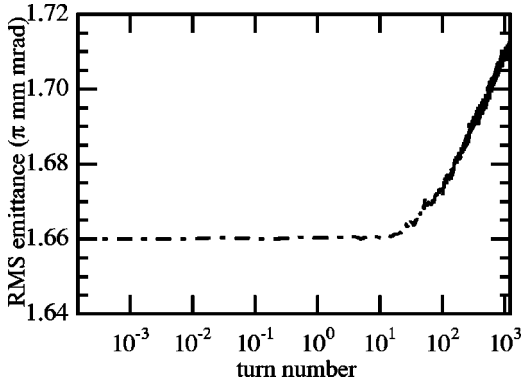

FIG. 4. RMS emittance growth of the mismatched waterbag beam.

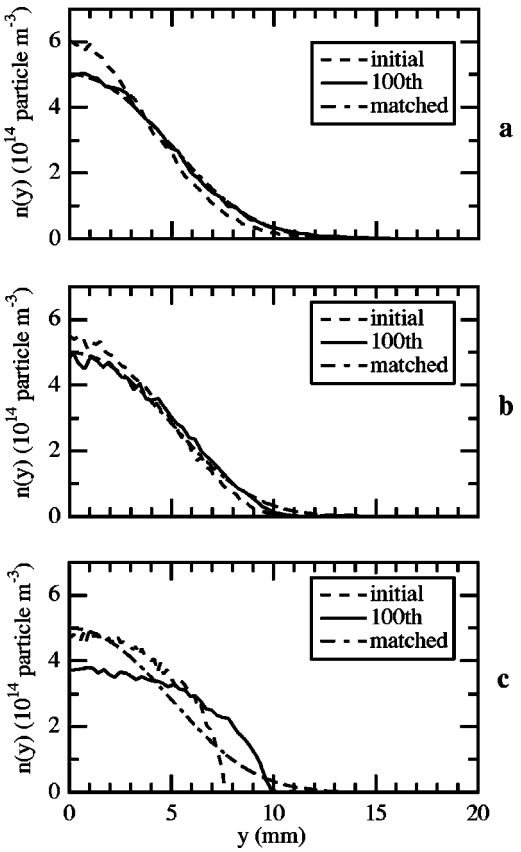

FIG. 5. Beam-density profile for three initial distributions: (a) Gaussian, (b) square-cosine, and (c) waterbag. The dashed and solid lines denote the initial state and 100th turn, respectively, and the dashed and single-dotted lines represent the Vlasov's solution of Fig. 2.

Since there are no external nonlinear fields in the uniform focusing channel, the sources driving the nonlinear resonances have been identified to be the space-charge self-fields. The simulation results also show a notable oscillation of the rms beam size as shown in Fig. 8, which is simply induced by mismatching. A parametric resonance between the single-particle motion and the rms beam core oscillation can be excited when the depressed betatron tune ν_β and the rms core oscillation tune ν_c satisfy $\nu_\beta/\nu_c=i/j$, where i and j are integers [7]. The lowest dominating resonance is obviously a second-harmonic resonance which is capable of creating two resonance islands as shown in Fig. 6. Certainly, the FFT of the core oscillation exhibits a single sharp peak at $\nu_c=10.45$ as shown in Fig. 9. The results strongly suggest that the major source of the second-harmonic resonance is the rms beam core oscillation.

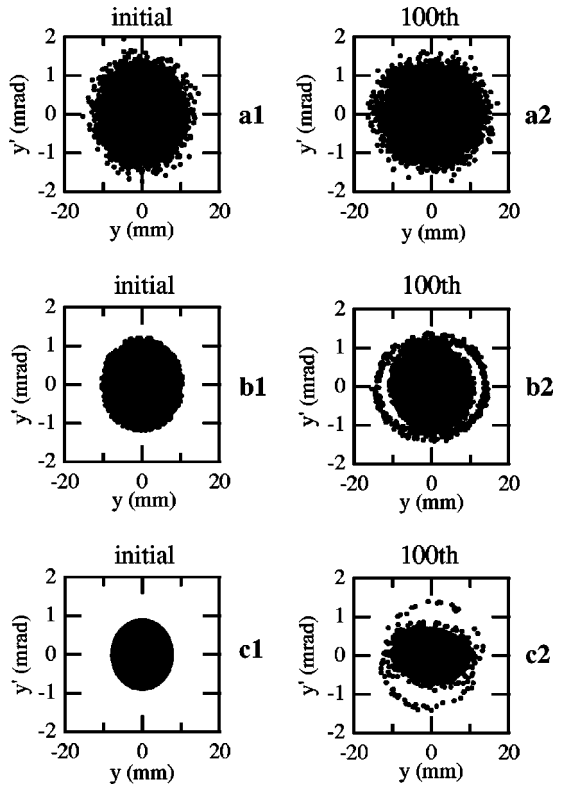

FIG. 6. Phase-space projections of mismatched beams at the initial condition (left) and 100th turn (right). (a) Gaussian, (b) square-cosine, and (c) waterbag.

IV. NONLINEAR RESONANCE EXCITED BY BEAM-CORE OSCILLATION

In order to confirm the speculation suggested by the simulation results that the rms beam-core oscillation is capable of driving the second-harmonic resonance, we have developed an analytic approach using an isolated resonance Hamiltonian. Here, the beam distribution is assumed to be a Gaussian distribution with the rms beam size oscillating at a single frequency. This is $\sigma(s)=\sigma_0[1+\delta\cos(\omega_c s)]$, where σ_0 is the averaged rms beam size, δ is the maximum deviation from σ_0, and $\omega_c=2\pi\nu_c/C$ is the frequency of the beam-core oscillation. Then the Gaussian distribution in the rest frame is given by $n(y,s)=N_0\exp[-y^2/\{2\sigma(s)^2\}]/\{\sqrt{2\pi}\sigma(s)\}$, where N_0 is the total number of particles per unit length in the rest frame. The electric field of this beam associated with the charge density is written in the form of a Taylor expansion $E_y(y,s)=eN_0\Sigma_{n=0}^{\infty}(-1)^n y^{2n+1}/\{\epsilon_0\sqrt{2\pi}n!(2n+1)2^n\sigma(s)^{2n+1}\}$. The original perturbed betatron equation (2.2) is rewritten as

$$y''+\omega_\beta^2 y=A_0\sum_{n=0}^{\infty}\frac{(-1)^n}{n!(2n+1)2^n}\frac{y^{2n+1}}{\sigma(s)^{2n+1}}, \qquad (4.1)$$

where $A_0=e^2N_0/\{\gamma^2\epsilon_0 mv^2\sqrt{2\pi}\}$. Introducing action-angle variables (ϕ,J), where $y=\sqrt{2J/\omega_0}\cos\phi$ and $p=\sqrt{2\omega_0 J}\sin\phi$, the Hamiltonian equivalent to Eq. (4.1) is expressed as

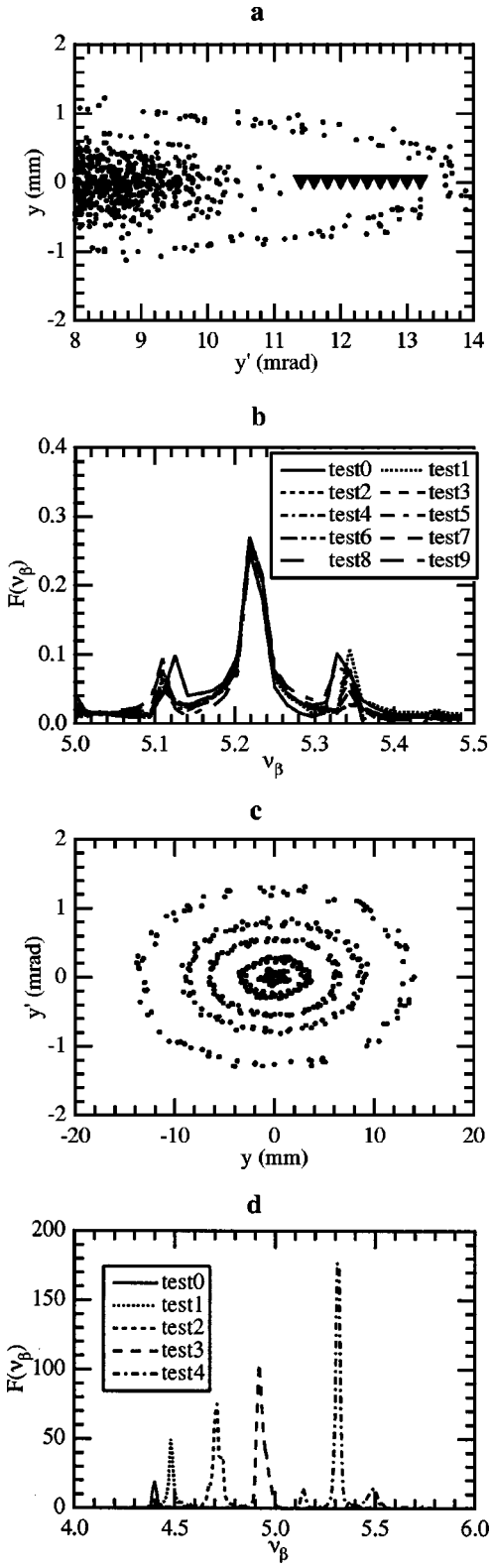

FIG. 7. (a) Position (solid triangle) and (b) frequency spectra of the test particles. (c) The Poincaré map and (d) the frequency spectra of nonresonant particles.

$$H=\omega_\beta J-A_0\sum_{n=0}^{\infty}\frac{(-1)^n}{n!(2n+2)(2n+1)2^n\sigma_0^{2n+1}}\times\left(\frac{2J}{\omega_\beta}\right)^{n+1}F_n(\phi,s), \qquad (4.2)$$

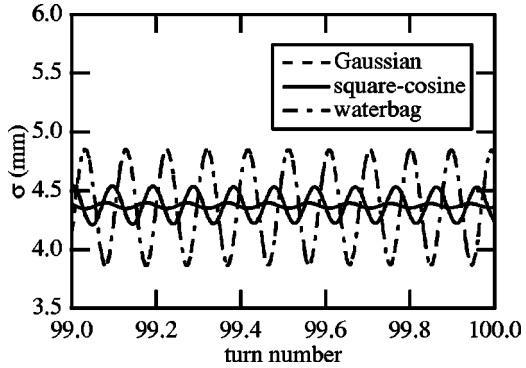

FIG. 8. σ of mismatched beams.

where

$$F_n(\phi,s)=\frac{\cos^{2n+2}\phi}{[1+\delta\cos(\omega_c s)]^{2n+1}}. \tag{4.3}$$

In the case of interest, where $\delta \ll 1$, Eq. (4.3) is approximated by

$$F_n(\phi,s)=[1-(2n+1)\delta\cos(\omega_c s)]\cos^{2n+2}\phi. \tag{4.4}$$

Here, $\cos(\omega_c s)\cos^{2n+2}\phi$ in Eq. (4.4) is decomposed in terms of $\cos(2l\phi \pm \omega_c s)$, where l is an integer. The second-harmonic resonance is excited in the case that the phase of Eq. (4.4) slowly varies with s. Because the second-harmonic resonance of the simulation result is excited in the case of $\nu_\beta/\nu_c=1/2$, it is found that the slowly oscillating phase is $2\phi-\omega_c s$. The rapidly oscillating terms, except for the terms including $2\phi-\omega_c s$, disappear after averaging the Hamiltonian of Eq. (4.2) over many turns [5]. The averaged Hamiltonian is called the isolated resonance Hamiltonian. A canonical transformation from (ϕ,J) to (ψ,J), where $\psi=\phi-\omega_c s/2$ is physically a rotation in phase space, is made to remove any time dependence from the isolated resonance Hamiltonian. The isolated resonance Hamiltonian H_{iso} is written as

$$H_{iso}=\left(\omega_\beta-\frac{\omega_c}{2}\right)J-2\sigma_0 A_0\sum_{n=0}^{\infty}a(n)J^{n+1} \times\left[\frac{1}{n+1}-\frac{2n+1}{n+2}\delta\cos(2\psi)\right], \tag{4.5}$$

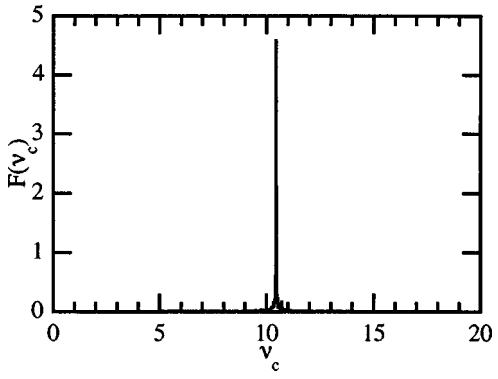

FIG. 9. Frequency spectrum of the rms beam core oscillation after arriving at a steady state.

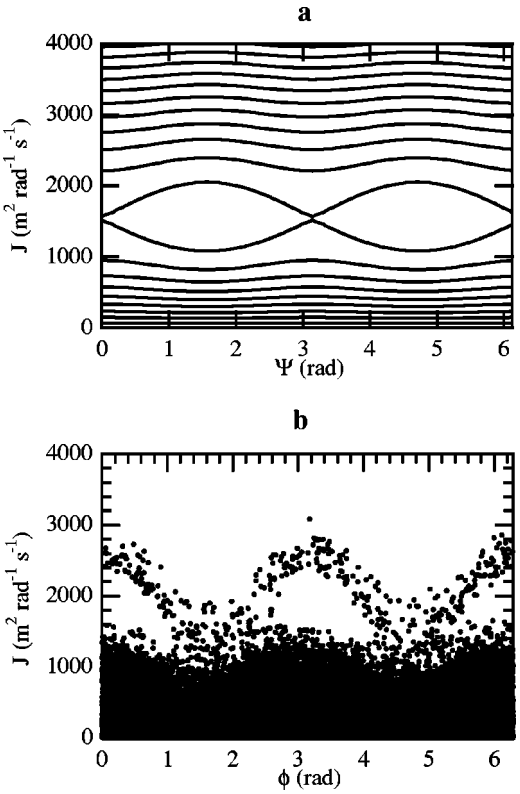

FIG. 10. (a) Contour plot of the Hamiltonian (10). (b) Simulation result of Fig. 6 exhibited in the action-angle space. $\sigma_0=4.38$ mm corresponds to $J=251.2$ m^2 rad^{-1} s^{-1} at $\phi=0$ rad.

where $a(n)=-(2n)!(n!)^{-3}(n+1)^{-1}(-4\sigma_0^2\omega_\beta)^{-n-1}$. The derivation is given in the Appendix.

A contour plot of the Hamiltonian (4.5) is shown in Fig. 10. The values of ω_0, σ_0, and δ at the steady state are chosen based on the simulation results for the case of an initial square-cosine beam. Two resonance islands are shown clearly. The position and size of the resonance islands are well known to be a good measure of the relative strength of perturbing terms. We evaluate these parameters from the beam parameters and the machine parameters. For this purpose, we will find the stable fixed and unstable fixed points of this nonlinear system. The stable fixed points at $\psi=\pi/2$ and $3\pi/2$ rad and the unstable fixed point at $\psi=0$ and π rad are analytically evaluated from the canonical equations $d\psi/dt=\partial H/\partial J=0$ and $dJ/dt=-\partial H/\partial\psi=0$. The maximum and minimum values of the action variable along

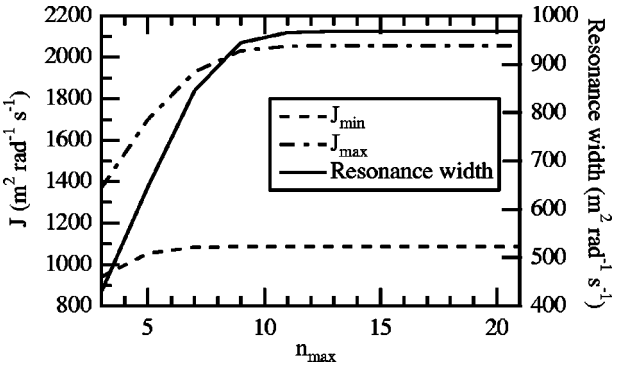

FIG. 11. $J_{\max}$, $J_{\min}$ and resonance width vs $n_{\max}$.

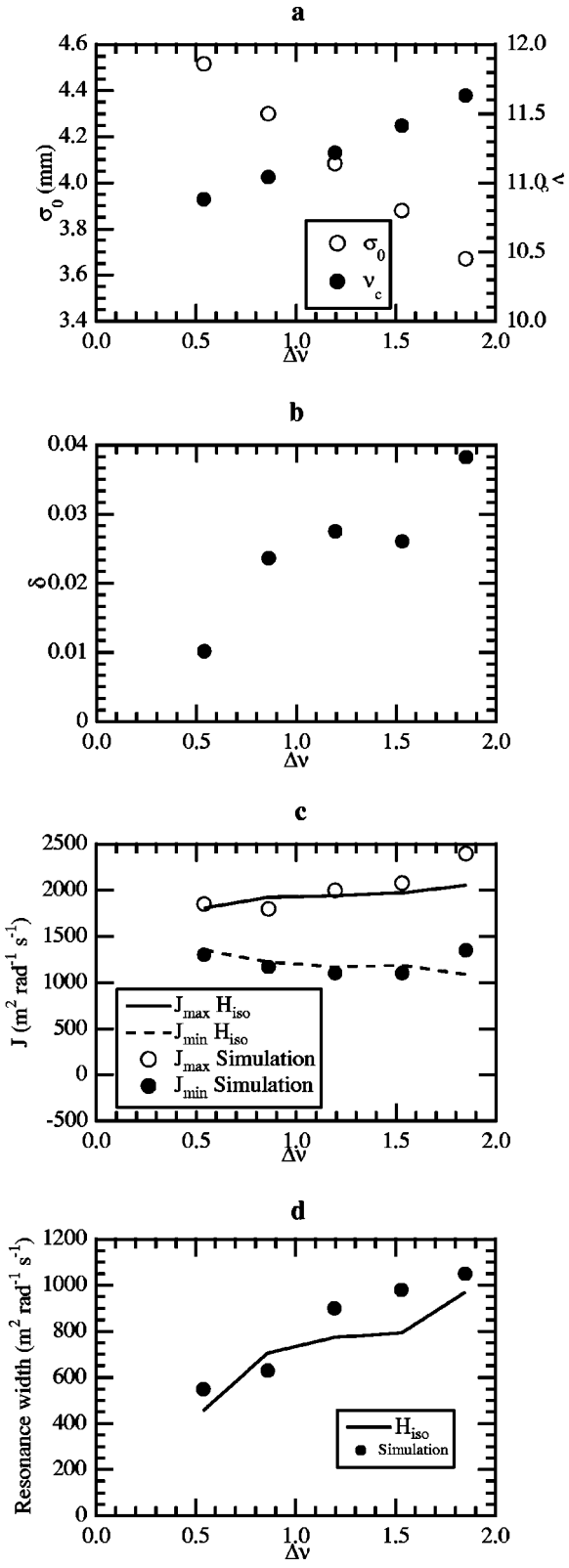

FIG. 12. (a) σ_0 and ν_c vs $\Delta\nu$. (b) δ vs $\Delta\nu$. (c) $J_{\max}$ and $J_{\min}$ vs $\Delta\nu$. (d) Resonance width vs $\Delta\nu$.

the trajectory through the unstable fixed point are defined as $J_{\max}$ and $J_{\min}$, respectively. The size of the resonance island (resonance width) is given by $J_{\max}-J_{\min}$ on the action axis.

In order to obtain a necessary and sufficient limit $n_{\max}$ in summation of Eq. (4.5), the values of $J_{\max}$, $J_{\min}$ and the resonance width were calculated as a function of $n_{\max}$. Its result is shown in Fig. 11. Also, $n_{\max}$ must be more than 11. A lower $n_{\max}$ gives the wrong results. Here, $n_{\max}=15$ has been applied.

Calculations of $J_{\max}$ and $J_{\min}$ are straightforwardly performed using the canonical equations, if the values of σ_0, ω_c, and δ at the steady state, which depend on the initial state, are given. The example of the simulation result shown in Figs. 12(a) and 12(b) was obtained assuming initial states with the same square-cosine distribution but with a different $\Delta\nu$. The $J_{\max}$ and $J_{\min}$ are calculated employing each set of the above parameters. The calculated locations of the resonance islands are in good agreement with the simulation results as shown in Figs. 12(c) and 12(d). We have reached the conclusion that the second-harmonic resonance is driven by the beam-core oscillation of the nearly Gaussian distribution. In addition, Fig. 10 clearly indicates that the outer edge of the resonance corresponds to the location of the halo.

V. CONCLUSION

Parametric interactions between a core oscillation and the highly nonlinear motion of individual particles drive the second-harmonic resonance for a 1D Gaussian distribution. This idea supports the speculation of Ref. [3] for a realistic beam distribution. The second-harmonic resonance is a source of emittance growth, which results in a beam halo at the outer edge of the resonance islands. The location of the halo is analytically tractable using canonical equations derived from the isolated resonance Hamiltonian. Nonlinearity in the particle motion is crucial in determining the location of the halo; the second-harmonic terms down-fed from higher order of the nonlinear terms are included in order to accurately estimate the halo location. An estimation of the halo location would provide a reasonable choice of the physical aperture or halo collimator in proposed high-intensity proton accelerators.

Applications of the developed analytic tool for a more realistic 2D distribution in periodic focusing seem to be straightforward. They will be discussed in forthcoming papers.

ACKNOWLEDGMENTS

One of the authors (Y.S.) would like to thank K. Ishibashi, K. Maehata, S. Kishiro, T. Toyama, M. Uota, and E. Nakamura for their useful comments throughout this study. He would like to thank F. Jones of TRIUMF for useful comments on the manuscript.

APPENDIX

In this appendix, we derive Eq. (4.5) from Eq. (4.2). In Eq. (4.4), the substitution

$$\cos^{2n+2}\theta=\frac{1}{2^{2n+2}}\binom{2n+2}{n+1}+\frac{1}{2^{2n+1}}\times\sum_{l=1}^{n}\binom{2n+2}{n-l+1}\cos(2l\theta) \qquad \text{(A1)}$$

gives

$$F_n(\phi,s)=\frac{1}{2^{2n+2}}\binom{2n+2}{n+1}-\frac{2n+1}{2^{2n+2}}\binom{2n+2}{n+1}\delta\cos(\omega_c s)$$
$$+\frac{1}{2^{2n+1}}\sum_{l=1}^{n}\binom{2n+2}{n-l+1}\cos(2l\phi)$$
$$-\frac{(2n+1)\delta}{2^{2n+2}}\sum_{l=1}^{n}\binom{2n+2}{n-l+1}\{\cos(2l\phi+\omega_c s)$$
$$+\cos(2l\phi-\omega_c s)\}. \tag{A2}$$

Thus, the time-averaged Hamiltonian is given by

$$\langle H\rangle=\omega_\beta J-A_0$$
$$\times\left\langle\sum_{n=0}^{\infty}\frac{(-1)^n}{n!(2n+2)(2n+1)2^n\sigma_0^{2n+1}}\left(\frac{2J}{\omega_\beta}\right)^{n+1}F_n(\phi,s)\right\rangle$$
$$=\omega_\beta J-A_0\sum_{n=0}^{\infty}\frac{(-1)^n J^{n+1}(2n)!}{(n!)^3(n+1)(2\sigma_0)^{2n+1}\omega_\beta^{n+1}}$$
$$\times\left[\frac{1}{n+1}-\delta\frac{2n+1}{n+2}\cos(2\phi-\omega_c s)\right]. \tag{A3}$$

Since $\langle H\rangle$ is not a constant of the motion, the canonical transformation from (ϕ,J) to (ψ,J) is made, where the generating function is $F_2=\psi J$. Thus, the isolated resonance Hamiltonian, Eq. (4.5), is obtained.

[1] H. Okamoto and M. Ikegami, Phys. Rev. E **55**, 4694 (1997).

[2] J. A. Holmes, J. D. Galambos, D. K. Olsen, and S. Y. Lee, in *Proceedings of the 1999 Particle Accelerator Conference*, edited by A. Luccio and W. Mackay (IEEE, New York, 1999), p. 279.

[3] R.L. Gluckstern, W. Cheng, S.S. Kurennoy, and H. Ye, Phys. Rev. E **54**, 6788 (1996).

[4] K. Takayama (unpublished).

[5] D.R. Douglas, in *Physics of Particle Accelerators*, edited by M. Month and M. Dienes, AIP Conf. Proc. No. 153 (AIP, New York, 1987).

[6] G. Franchetti, I. Hofmann, and G. Turchetti, Nucl. Instrum. Methods Phys. Res. A **415**, 450 (1998).

[7] M. Pabst, K. Bongardt, and A. Letchford, in *Proceedings of the 1999 Particle Accelerator Conference* (Ref. [2]), p. 146.